Cross section for $b\bar{b}$ production via dielectrons in d+Au collisions at $\sqrt{s_{NN}}$ =200 GeV

A. Adare,[13] C. Aidala,[41,42] N.N. Ajitanand,[58] Y. Akiba,[54,55] H. Al-Bataineh,[48] J. Alexander,[58] A. Angerami,[14] K. Aoki,[33,54] N. Apadula,[59] Y. Aramaki,[12,54] E.T. Atomssa,[34] R. Averbeck,[59] T.C. Awes,[50] B. Azmoun,[7] V. Babintsev,[23] M. Bai,[6] G. Baksay,[19] L. Baksay,[19] K.N. Barish,[8] B. Bassalleck,[47] A.T. Basye,[1] S. Bathe,[5,8,55] V. Baublis,[53] C. Baumann,[43] A. Bazilevsky,[7] S. Belikov,[7,*] R. Belmont,[63] R. Bennett,[59] J.H. Bhom,[67] D.S. Blau,[32] J.S. Bok,[67] K. Boyle,[59] M.L. Brooks,[37] H. Buesching,[7] V. Bumazhnov,[23] G. Bunce,[7,55] S. Butsyk,[37] S. Campbell,[59] A. Caringi,[44] C.-H. Chen,[59] C.Y. Chi,[14] M. Chiu,[7] I.J. Choi,[67] J.B. Choi,[10] R.K. Choudhury,[4] P. Christiansen,[39] T. Chujo,[62] P. Chung,[58] O. Chvala,[8] V. Cianciolo,[50] Z. Citron,[59] B.A. Cole,[14] Z. Conesa del Valle,[34] M. Connors,[59] M. Csanád,[17] T. Csörgő,[66] T. Dahms,[59] S. Dairaku,[33,54] I. Danchev,[63] K. Das,[20] A. Datta,[41] G. David,[7] M.K. Dayananda,[21] A. Denisov,[23] A. Deshpande,[55,59] E.J. Desmond,[7] K.V. Dharmawardane,[48] O. Dietzsch,[57] A. Dion,[27,59] M. Donadelli,[57] O. Drapier,[34] A. Drees,[59] K.A. Drees,[6] J.M. Durham,[37,59] A. Durum,[23] D. Dutta,[4] L. D'Orazio,[40] S. Edwards,[20] Y.V. Efremenko,[50] F. Ellinghaus,[13] T. Engelmore,[14] A. Enokizono,[50] H. En'yo,[54,55] S. Esumi,[62] B. Fadem,[44] D.E. Fields,[47] M. Finger,[9] M. Finger, Jr.,[9] F. Fleuret,[34] S.L. Fokin,[32] Z. Fraenkel,[65,*] J.E. Frantz,[49,59] A. Franz,[7] A.D. Frawley,[20] K. Fujiwara,[54] Y. Fukao,[54] T. Fusayasu,[46] I. Garishvili,[60] A. Glenn,[36] H. Gong,[59] M. Gonin,[34] Y. Goto,[54,55] R. Granier de Cassagnac,[34] N. Grau,[2,14] S.V. Greene,[63] G. Grim,[37] M. Grosse Perdekamp,[24] T. Gunji,[12] H.-Å. Gustafsson,[39,*] J.S. Haggerty,[7] K.I. Hahn,[18] H. Hamagaki,[12] J. Hamblen,[60] R. Han,[52] J. Hanks,[14] E. Haslum,[39] R. Hayano,[12] X. He,[21] M. Heffner,[36] T.K. Hemmick,[59] T. Hester,[8] J.C. Hill,[27] M. Hohlmann,[19] W. Holzmann,[14] K. Homma,[22] B. Hong,[31] T. Horaguchi,[22] D. Hornback,[60] S. Huang,[63] T. Ichihara,[54,55] R. Ichimiya,[54] Y. Ikeda,[62] K. Imai,[28,33,54] M. Inaba,[62] D. Isenhower,[1] M. Ishihara,[54] M. Issah,[63] D. Ivanischev,[53] Y. Iwanaga,[22] B.V. Jacak,[59] J. Jia,[7,58] X. Jiang,[37] J. Jin,[14] B.M. Johnson,[7] T. Jones,[1] K.S. Joo,[45] D. Jouan,[51] D.S. Jumper,[1] F. Kajihara,[12] J. Kamin,[59] J.H. Kang,[67] J. Kapustinsky,[37] K. Karatsu,[33,54] M. Kasai,[54,56] D. Kawall,[41,55] M. Kawashima,[54,56] A.V. Kazantsev,[32] T. Kempel,[27] A. Khanzadeev,[53] K.M. Kijima,[22] J. Kikuchi,[64] A. Kim,[18] B.I. Kim,[31] D.J. Kim,[29] E.-J. Kim,[10] Y.-J. Kim,[24] E. Kinney,[13] Á. Kiss,[17] E. Kistenev,[7] D. Kleinjan,[8] L. Kochenda,[53] B. Komkov,[53] M. Konno,[62] J. Koster,[24] A. Král,[15] A. Kravitz,[14] G.J. Kunde,[37] K. Kurita,[54,56] M. Kurosawa,[54] Y. Kwon,[67] G.S. Kyle,[48] R. Lacey,[58] Y.S. Lai,[14] J.G. Lajoie,[27] A. Lebedev,[27] D.M. Lee,[37] J. Lee,[18] K.B. Lee,[31] K.S. Lee,[31] M.J. Leitch,[37] M.A.L. Leite,[57] X. Li,[11] P. Lichtenwalner,[44] P. Liebing,[55] L.A. Linden Levy,[13] T. Liška,[15] H. Liu,[37] M.X. Liu,[37] B. Love,[63] D. Lynch,[7] C.F. Maguire,[63] Y.I. Makdisi,[6] M.D. Malik,[47] V.I. Manko,[32] E. Mannel,[14] Y. Mao,[52,54] H. Masui,[62] F. Matathias,[14] M. McCumber,[59] P.L. McGaughey,[37] D. McGlinchey,[13,20] N. Means,[59] B. Meredith,[24] Y. Miake,[62] T. Mibe,[30] A.C. Mignerey,[40] K. Miki,[54,62] A. Milov,[7] J.T. Mitchell,[7] A.K. Mohanty,[4] H.J. Moon,[45] Y. Morino,[12] A. Morreale,[8] D.P. Morrison,[7,†] T.V. Moukhanova,[32] T. Murakami,[33] J. Murata,[54,56] S. Nagamiya,[30,54] J.L. Nagle,[13,‡] M. Naglis,[65] M.I. Nagy,[66] I. Nakagawa,[54,55] Y. Nakamiya,[22] K.R. Nakamura,[33,54] T. Nakamura,[54] K. Nakano,[54] S. Nam,[18] J. Newby,[36] M. Nguyen,[59] M. Nihashi,[22] R. Nouicer,[7] A.S. Nyanin,[32] C. Oakley,[21] E. O'Brien,[7] S.X. Oda,[12] C.A. Ogilvie,[27] M. Oka,[62] K. Okada,[55] Y. Onuki,[54] A. Oskarsson,[39] M. Ouchida,[22,54] K. Ozawa,[12] R. Pak,[7] V. Pantuev,[25,59] V. Papavassiliou,[48] I.H. Park,[18] S.K. Park,[31] W.J. Park,[31] S.F. Pate,[48] H. Pei,[27] J.-C. Peng,[24] H. Pereira,[16] D.Yu. Peressounko,[32] R. Petti,[59] C. Pinkenburg,[7] R.P. Pisani,[7] M. Proissl,[59] M.L. Purschke,[7] H. Qu,[21] J. Rak,[29] I. Ravinovich,[65] K.F. Read,[50,60] S. Rembeczki,[19] K. Reygers,[43] V. Riabov,[53] Y. Riabov,[53] E. Richardson,[40] D. Roach,[63] G. Roche,[38] S.D. Rolnick,[8] M. Rosati,[27] C.A. Rosen,[13] S.S.E. Rosendahl,[39] P. Ružička,[26] B. Sahlmueller,[43,59] N. Saito,[30] T. Sakaguchi,[7] K. Sakashita,[54,61] V. Samsonov,[53] S. Sano,[12,64] T. Sato,[62] S. Sawada,[30] K. Sedgwick,[8] J. Seele,[13] R. Seidl,[24,55] R. Seto,[8] D. Sharma,[65] I. Shein,[23] T.-A. Shibata,[54,61] K. Shigaki,[22] M. Shimomura,[62] K. Shoji,[33,54] P. Shukla,[4] A. Sickles,[7] C.L. Silva,[27] D. Silvermyr,[50] C. Silvestre,[16] K.S. Sim,[31] B.K. Singh,[3] C.P. Singh,[3] V. Singh,[3] M. Slunečka,[9] R.A. Soltz,[36] W.E. Sondheim,[37] S.P. Sorensen,[60] I.V. Sourikova,[7] P.W. Stankus,[50] E. Stenlund,[39] S.P. Stoll,[7] T. Sugitate,[22] A. Sukhanov,[7] J. Sziklai,[66] E.M. Takagui,[57] A. Taketani,[54,55] R. Tanabe,[62] Y. Tanaka,[46] S. Taneja,[59] K. Tanida,[33,54,55] M.J. Tannenbaum,[7] S. Tarafdar,[3] A. Taranenko,[58] H. Themann,[59] D. Thomas,[1] T.L. Thomas,[47] M. Togawa,[55] A. Toia,[59] L. Tomášek,[26] H. Torii,[22] R.S. Towell,[1] I. Tserruya,[65] Y. Tsuchimoto,[22] C. Vale,[7] H. Valle,[63] H.W. van Hecke,[37] E. Vazquez-Zambrano,[14] A. Veicht,[24] J. Velkovska,[63] R. Vértesi,[66] M. Virius,[15] V. Vrba,[26] E. Vznuzdaev,[53] X.R. Wang,[48] D. Watanabe,[22] K. Watanabe,[62] Y. Watanabe,[54,55] F. Wei,[27] R. Wei,[58] J. Wessels,[43] S.N. White,[7] D. Winter,[14] C.L. Woody,[7] R.M. Wright,[1] M. Wysocki,[13] Y.L. Yamaguchi,[12,54] K. Yamaura,[22] R. Yang,[24] A. Yanovich,[23] J. Ying,[21] S. Yokkaichi,[54,55] Z. You,[52] G.R. Young,[50] I. Younus,[35,47] I.E. Yushmanov,[32] W.A. Zajc,[14] and S. Zhou[11]

(PHENIX Collaboration)

[1]Abilene Christian University, Abilene, Texas 79699, USA
[2]Department of Physics, Augustana College, Sioux Falls, South Dakota 57197, USA
[3]Department of Physics, Banaras Hindu University, Varanasi 221005, India
[4]Bhabha Atomic Research Centre, Bombay 400 085, India
[5]Baruch College, City University of New York, New York, New York, 10010 USA
[6]Collider-Accelerator Department, Brookhaven National Laboratory, Upton, New York 11973-5000, USA
[7]Physics Department, Brookhaven National Laboratory, Upton, New York 11973-5000, USA
[8]University of California - Riverside, Riverside, California 92521, USA
[9]Charles University, Ovocný trh 5, Praha 1, 116 36, Prague, Czech Republic
[10]Chonbuk National University, Jeonju, 561-756, Korea
[11]Science and Technology on Nuclear Data Laboratory, China Institute of Atomic Energy, Beijing 102413, P. R. China
[12]Center for Nuclear Study, Graduate School of Science, University of Tokyo, 7-3-1 Hongo, Bunkyo, Tokyo 113-0033, Japan
[13]University of Colorado, Boulder, Colorado 80309, USA
[14]Columbia University, New York, New York 10027 and Nevis Laboratories, Irvington, New York 10533, USA
[15]Czech Technical University, Zikova 4, 166 36 Prague 6, Czech Republic
[16]Dapnia, CEA Saclay, F-91191, Gif-sur-Yvette, France
[17]ELTE, Eötvös Loránd University, H - 1117 Budapest, Pázmány P. s. 1/A, Hungary
[18]Ewha Womans University, Seoul 120-750, Korea
[19]Florida Institute of Technology, Melbourne, Florida 32901, USA
[20]Florida State University, Tallahassee, Florida 32306, USA
[21]Georgia State University, Atlanta, Georgia 30303, USA
[22]Hiroshima University, Kagamiyama, Higashi-Hiroshima 739-8526, Japan
[23]IHEP Protvino, State Research Center of Russian Federation, Institute for High Energy Physics, Protvino, 142281, Russia
[24]University of Illinois at Urbana-Champaign, Urbana, Illinois 61801, USA
[25]Institute for Nuclear Research of the Russian Academy of Sciences, prospekt 60-letiya Oktyabrya 7a, Moscow 117312, Russia
[26]Institute of Physics, Academy of Sciences of the Czech Republic, Na Slovance 2, 182 21 Prague 8, Czech Republic
[27]Iowa State University, Ames, Iowa 50011, USA
[28]Advanced Science Research Center, Japan Atomic Energy Agency, 2-4
Shirakata Shirane, Tokai-mura, Naka-gun, Ibaraki-ken 319-1195, Japan
[29]Helsinki Institute of Physics and University of Jyväskylä, P.O.Box 35, FI-40014 Jyväskylä, Finland
[30]KEK, High Energy Accelerator Research Organization, Tsukuba, Ibaraki 305-0801, Japan
[31]Korea University, Seoul, 136-701, Korea
[32]Russian Research Center "Kurchatov Institute", Moscow, 123098 Russia
[33]Kyoto University, Kyoto 606-8502, Japan
[34]Laboratoire Leprince-Ringuet, Ecole Polytechnique, CNRS-IN2P3, Route de Saclay, F-91128, Palaiseau, France
[35]Physics Department, Lahore University of Management Sciences, Lahore 54792, Pakistan
[36]Lawrence Livermore National Laboratory, Livermore, California 94550, USA
[37]Los Alamos National Laboratory, Los Alamos, New Mexico 87545, USA
[38]LPC, Université Blaise Pascal, CNRS-IN2P3, Clermont-Fd, 63177 Aubiere Cedex, France
[39]Department of Physics, Lund University, Box 118, SE-221 00 Lund, Sweden
[40]University of Maryland, College Park, Maryland 20742, USA
[41]Department of Physics, University of Massachusetts, Amherst, Massachusetts 01003-9337, USA
[42]Department of Physics, University of Michigan, Ann Arbor, Michigan 48109-1040, USA
[43]Institut fur Kernphysik, University of Muenster, D-48149 Muenster, Germany
[44]Muhlenberg College, Allentown, Pennsylvania 18104-5586, USA
[45]Myongji University, Yongin, Kyonggido 449-728, Korea
[46]Nagasaki Institute of Applied Science, Nagasaki-shi, Nagasaki 851-0193, Japan
[47]University of New Mexico, Albuquerque, New Mexico 87131, USA
[48]New Mexico State University, Las Cruces, New Mexico 88003, USA
[49]Department of Physics and Astronomy, Ohio University, Athens, Ohio 45701, USA
[50]Oak Ridge National Laboratory, Oak Ridge, Tennessee 37831, USA
[51]IPN-Orsay, Universite Paris Sud, CNRS-IN2P3, BP1, F-91406, Orsay, France
[52]Peking University, Beijing 100871, P. R. China
[53]PNPI, Petersburg Nuclear Physics Institute, Gatchina, Leningrad region, 188300, Russia
[54]RIKEN Nishina Center for Accelerator-Based Science, Wako, Saitama 351-0198, Japan
[55]RIKEN BNL Research Center, Brookhaven National Laboratory, Upton, New York 11973-5000, USA
[56]Physics Department, Rikkyo University, 3-34-1 Nishi-Ikebukuro, Toshima, Tokyo 171-8501, Japan
[57]Universidade de São Paulo, Instituto de Física, Caixa Postal 66318, São Paulo CEP05315-970, Brazil
[58]Chemistry Department, Stony Brook University, SUNY, Stony Brook, New York 11794-3400, USA
[59]Department of Physics and Astronomy, Stony Brook University, SUNY, Stony Brook, New York 11794-3800,, USA
[60]University of Tennessee, Knoxville, Tennessee 37996, USA
[61]Department of Physics, Tokyo Institute of Technology, Oh-okayama, Meguro, Tokyo 152-8551, Japan
[62]Institute of Physics, University of Tsukuba, Tsukuba, Ibaraki 305, Japan
[63]Vanderbilt University, Nashville, Tennessee 37235, USA

[64] Waseda University, Advanced Research Institute for Science and Engineering, 17 Kikui-cho, Shinjuku-ku, Tokyo 162-0044, Japan
[65] Weizmann Institute, Rehovot 76100, Israel
[66] Institute for Particle and Nuclear Physics, Wigner Research Centre for Physics, Hungarian Academy of Sciences (Wigner RCP, RMKI) H-1525 Budapest 114, POBox 49, Budapest, Hungary
[67] Yonsei University, IPAP, Seoul 120-749, Korea

(Dated: May 19, 2014)

We report a measurement of e^+e^- pairs from semileptonic heavy-flavor decays in d+Au collisions at $\sqrt{s_{NN}}$ = 200 GeV. Exploring the mass and transverse-momentum dependence of the yield, the bottom decay contribution can be isolated from charm, and quantified by comparison to PYTHIA and MC@NLO simulations. The resulting $b\bar{b}$-production cross section is $\sigma_{b\bar{b}}^{d\mathrm{Au}}$ = 1.37±0.28(stat)±0.46(syst) mb, which is equivalent to a nucleon-nucleon cross section of σ_{bb}^{NN} = 3.4 ± 0.8(stat)±1.1(syst) μb.

PACS numbers: 25.75.Dw

I. INTRODUCTION

Collisions of heavy nuclei at the Relativistic Heavy Ion Collider (RHIC) at Brookhaven National Laboratory produce a quark-gluon plasma, which is a fundamentally new strongly coupled state of partonic matter [1–4]. There is extensive experimental evidence that partons lose energy while traversing the hot medium [5–7]. Many theoretical studies have been performed to determine the role of gluon radiation and collisional energy loss processes [8, 9], as well as to confront the data with predictions based upon AdS/CFT [10].

The fate of a higher mass quark traversing the plasma can help elucidate the mechanism of the energy loss, as the quark mass affects gluon radiation in the medium [11]. Consequently, single electrons and positrons from the decays of mesons containing heavy quarks have been studied in various systems at both RHIC [12–14] and the Large Hadron Collider at CERN [15, 16].

Differentiating among theoretical descriptions of the energy loss will be aided by comparing charm and bottom yields. In order to observe quark-gluon plasma effects on heavy quarks, it is crucial to compare Au+Au data to a baseline measurement not dominated by the plasma. Typically p+p collisions are used to provide this baseline. There are also effects of cold nuclear matter on the production of heavy quarks, which can be studied by comparing p+p to p+Pb or d+Au. PHENIX has already reported modification in cold nuclear matter of single electrons at moderate p_T [13], heavy flavor measured through e-μ correlations [17] and J/ψ [18, 19]. Of course, the bound state can be broken up in cold nuclear matter, so the $c\bar{c}$ and $b\bar{b}$ production cross sections in d+Au are of interest.

Clean c/b separation is difficult to achieve with single lepton measurements, as the single lepton spectrum contains both charm and bottom contributions. The B decay contribution increases with p_T, and is comparable to the D decay contribution at $p_T \geq 3$ GeV/c [20, 21]. PHENIX performed initial measurements of the charm and bottom cross sections in p+p collisions via high mass dielectrons [22] and electron-hadron correlations [20]. STAR also reported a $b\bar{b}$ cross section in p+p collisions [14] measured through single electron spectra.

Reconstructing heavy flavor hadrons or measuring leptons with displaced vertices allows more direct separation of charm and bottom. However, such measurements require microvertex detectors or large data sets into a very large aperture with high resolution hadron identification. PHENIX has a new silicon microvertex detector, but no d+Au data have been collected with it yet.

Dielectron spectra, which are double differential in mass and p_T, allow separation of regions dominated by charm from those dominated by bottom. The yield and shape of the mass and p_T spectra provide sensitivity to the heavy flavor cross sections. Furthermore, the spectra can also encode information about the heavy flavor production mechanism via the dielectron correlations, which affect the detected pair mass and p_T and therefore the spectral shape.

Initial-state effects such as gluon shadowing in the nucleus may affect heavy quark cross sections as the dominant production channel at RHIC is gluon fusion. The shape of the mass and p_T distributions of charm and bottom decay electrons could additionally be sensitive to other effects, such as parton energy loss and rescattering in cold nuclear matter, for which evidence was recently reported [13]. While azimuthal correlations of the two leptons have advantages for studying the heavy-quark production process [17], analysis of dileptons as a function of mass and p_T is undertaken in order to separate charm and bottom contributions.

In this paper we report a high statistics measurement of dielectrons in d+Au collisions in order to provide part of the necessary baseline information for quark-gluon plasma studies. Section II describes the experimental apparatus and trigger. Section III presents details about

*Deceased
†PHENIX Co-Spokesperson: morrison@bnl.gov
‡PHENIX Co-Spokesperson: jamie.nagle@colorado.edu

the data analysis, including electron identification, background subtraction, and efficiency corrections. The data are presented in Section IV, as double differential spectra in mass and p_T. Expected sources of dielectrons, and effects of the PHENIX acceptance are also discussed in this section. In Section V the results are compared to models of charm and bottom production to determine the heavy flavor cross sections and examine sensitivity to leading-order and next-to-leading-order quantum chromodynamics (QCD) descriptions of heavy-flavor physics. Section VI presents our summary and conclusions.

II. EXPERIMENT

The data reported in this paper were collected in the 2008 RHIC d+Au run. The data were recorded by the PHENIX detector using both a minimum bias trigger and an electron trigger. A total of 3.1 billion triggered events were analyzed, corresponding to 116.6 billion sampled minimum bias events and an integrated luminosity of 58.6 $n\mathrm{b}^{-1}$ (equivalent to a nucleon-nucleon $\int Ldt = 23\ p\mathrm{b}^{-1}$).

Electrons are measured in PHENIX using the two central arm spectrometers, each covering $|\eta| < 0.35$ and $\Delta\phi = \pi/2$. A detailed description of the PHENIX detector is available in [23]. Tracks are reconstructed using information from hits in the drift chambers (DC) and pad chambers. The magnitude of the particle's bend in the central axial magnetic field is determined from the reconstructed track and used to determine the track's momentum. The momentum resolution for this data set is $\delta p/p = 0.011 \oplus 0.0116p$, where p is in GeV/$c$.

Tracks are projected onto the photomultiplier tube plane of the ring-imaging Čerenkov counter (RICH). Matched hits allow cuts on the ring shape and size to separate electrons from hadrons to approximately 5 GeV/c. The electromagnetic calorimeters (EMCal) measure the deposited energy and the shower shape. The ratio of the measured energy and momentum provides further electron identification [12].

The collision vertex, collision time, and minimum bias trigger are provided by a pair of beam-beam counters (BBC) located 144 cm from the center of PHENIX, on either side of the collision region. Each BBC comprises 64 quartz Čerenkov counters and covers a rapidity range of $3.0 < |\eta| < 3.9$. The collision vertex resolution is approximately 0.5 cm in d+Au collisions. The minimum bias trigger requires a coincidence between North and South sides of the BBC, with at least one hit on each side and accepts the events if the BBC vertex is within 38 cm of the nominal interaction vertex. The minimum bias trigger is sensitive to $88 \pm 4\%$ of all d+Au collisions [24].

Collisions producing an electron-positron pair are extremely rare; fewer than 1% of minimum bias triggered events contain a single electron (p_T >200 MeV) in the central arm acceptance. Consequently, pairs exist in only a tiny fraction of the events. Furthermore, pairs at high mass and high p_T have cross sections many orders of magnitude smaller than pairs from vector meson decays. As a result, electron triggered events are crucial for collecting a high statistics dielectron sample in d+Au. The PHENIX electron trigger requires a Čerenkov ring deposited in the RICH that is spatially aligned with a shower in the EMCal with energy above two thresholds of 600 and 800 MeV. The bias of the resulting samples is corrected for the trigger efficiency using the ratio of electron triggered to minimum bias triggered events as a function of electron momentum. The minimum bias triggered data sample does not require any minimum energy threshold criterion. The single electron trigger threshold creates a mass threshold for electron pairs, and is corrected by comparing to minimum bias collisions double-differentially in mass and p_T.

III. DATA ANALYSIS

Data quality cuts include fiducial cuts to remove any detector edge effects or dead areas. The data were collected into run groups with similar detector performance characteristics. Each group was analyzed separately, and the groups were combined after efficiency correction.

A. Electron identification

Electron candidates must pass track reconstruction quality cuts, have $p_T > 0.2$ GeV/c, as well as fire the RICH and EMCal detectors. To be identified as an electron, each candidate must be associated with two or more fired RICH photomultiplier tubes within the expected RICH ring size and position. In the relatively low multiplicity d+Au collisions, this is the main discriminating cut using the RICH. Electrons are also required to have a good match to an EMCal cluster. For further electron identification, the energy in the EMCal must satisfy the requirement $E/p > 0.5$. The electron purity is approximately 85-90%. Finally, to fully control the kinematic edge of the single electron p_T cut, the pair $m_T = \sqrt{m^2 + p_T^2}$ is required to be greater than 450 MeV/c.

Photon conversions in detector support structures are identified in the two-dimensional plane of DC hit azimuthal angle vs. E/p. Conversion electrons traverse a portion of the magnetic field and, consequently, their momentum and, therefore, their E/p is mismeasured. Fully reconstructed conversions in the beam pipe and air before the DC are removed by a cut on a pairwise variable, ϕ_V, defined as

$$\vec{u} = \frac{\vec{p}_1 + \vec{p}_2}{|\vec{p}_1 + \vec{p}_2|}, \quad (1)$$

$$\vec{v} = \vec{p}_1 \times \vec{p}_2, \quad (2)$$

$$\vec{w} = \vec{u} \times \vec{v}, \quad (3)$$

$$\vec{u}_a = \frac{\vec{u} \times \hat{z}}{|\vec{u} \times \hat{z}|}, \quad (4)$$

$$\phi_V = \arccos\left(\frac{\vec{w} \cdot \vec{u}_a}{|\vec{w}||\vec{u}_a|}\right). \quad (5)$$

Here $\vec{p}_1$ is the 3-momentum vector of the electron and $\vec{p}_2$ the 3-momentum vector of the positron. This is a cut on the orientation of the plane defined by the opening angle of the pair with respect to the magnetic field, which is parallel to the beam axis $\vec{z}$. The e^+e^- pairs from photon conversions have no intrinsic opening angle. Therefore, the only way they can be separated from each other is by the magnetic field pulling them apart. In this case, the opening angle will be aligned perpendicular to the magnetic field. However, any pair that decays from a source with mass must have an opening angle that is randomly oriented with respect to the magnetic field. For m_{ee} <600 MeV/c^2, this cut removes 98% of the conversions while retaining 80% of the signal pairs. At higher pair mass where the heavy flavor spectrum dominates, conversions are negligible and this cut does not affect the signal efficiency.

An additional source of contamination in the dielectron spectrum is due to hadron tracks that share a RICH ring with an electron. The sharing cannot be properly reproduced by event-mixing, so this contamination must be removed before background subtraction. As like-sign electron-hadron pairs populate a different region in mass and p_T from unlike-sign pairs, like-sign subtraction also cannot be used to remove this contamination. Consequently, a cut is placed on the distance between the projection of any two tracks onto the RICH photomultiplier tube plane. If the projections are within 10 σ in $\Delta\phi_{\rm RICH} \oplus \Delta z_{\rm RICH}$ (this corresponds $\approx$ 36 cm, roughly twice the predicted maximum diameter of a RICH ring), then the entire event is rejected. This cut does not affect the mass spectrum above $m_{ee} > 600$ MeV/c^2 and removes less than 1% of the events.

B. Background Subtraction

All electrons and positrons in a given event are combined into pairs. We refer to these as *foreground* and denote the number of e^+e^- pairs as N_{+-} and the like-sign pairs as $N_{\pm\pm}$. The foreground pairs contain signal pairs (S_{+-}) from the sources that we are interested in, and background pairs. Electrons and positrons from different physical sources ($B^{\rm comb}_{+-}$) are uncorrelated. Additionally, there are some e^+e^- background pairs which are correlated ($B^{\rm cor}_{+-}$), described in Section III B 1. Both types of background are subtracted statistically from the foreground to extract the signal.

Since the background is typically larger than the signal, the background estimation requires precision of a few percent. The signal-to-background (S/B) ratio varies with invariant mass of the pairs. In d+Au collisions, the p_T integrated S/B is larger than 1.0 only near the vector meson masses. It is below 0.1 for the low mass continuum (<1.0 GeV/c^2). In the intermediate mass continuum (1.0-3.0 GeV/c^2), the S/B is roughly constant between 0.2-0.3; the S/B increases for higher mass.

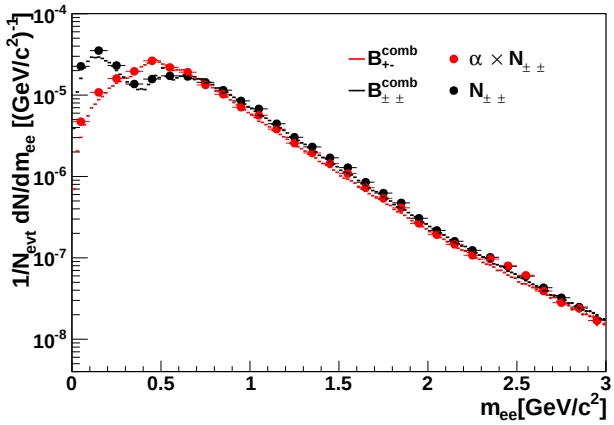

FIG. 1: Mass distribution for the combinatorial background determined by event mixing $B^{\rm comb}_{+-}$ and $B^{\rm comb}_{\pm\pm}$as the red and black line, respectively. The shape difference due to the difference in acceptance between like-sign and unlike-sign pairs in PHENIX is clearly visible. Also shown are foreground like-sign pairs $N_{\pm\pm}$(black points) and $N_{\pm\pm}$corrected for the acceptance difference (red points). The differences between points and lines are the the correlated background.

There are two different approaches to estimating the background, (i) the like-sign subtraction technique based on the measured like-sign foreground $N_{\pm\pm}$ or (ii) the event mixing technique. In the PHENIX experiment the acceptance for like and unlike-sign pairs is different due to the two arm geometry and thus the shape of the invariant mass distributions are different as illustrated in Figure 1. We therefore traditionally have used the event mixing technique. In this method, combinatorial background is estimated by taking an electron from event i and pairing it with a positron from event $j(\neq i)$. This is a powerful approach as it allows for an extremely high statistics estimation of the background [25]. However, such an estimation must be normalized with a precision much better than the S/B. In addition, the mixed event spectra do not contain any of the correlated background and therefore these additional pairs must be estimated using Monte Carlo methods.

In this paper we use the like-sign subtraction technique, which avoids the complications inherent in the mixed event background estimation. This method uses the acceptance difference for like and unlike-sign pairs, described in Section III B 2.

1. *Correlated Background*

There are two sources of correlated background: *cross pairs* and *jet pairs* [22]. Cross pairs are correlated

through a hadron decay that results in two e^+e^- pairs. These pairs originate from π^0 and η^0 double-Dalitz decays ($\pi^0(\eta) \rightarrow \gamma^*\gamma^* \rightarrow e^+e^-e^+e^-$), a single-Dalitz decay accompanied by a photon conversion ($\pi^0(\eta) \rightarrow \gamma\gamma^* \rightarrow e^+e^-e^+e^-$), and diphoton decays with both photons converting ($\pi^0(\eta) \rightarrow \gamma\gamma \rightarrow e^+e^-e^+e^-$). The cross pair correlation arises because of the small opening angle between the virtual and/or real decay photons. The resulting dielectrons tend to manifest at low mass and high p_T.

Jet pairs are the other major source of correlated e^+e^- background. In this case, the electron and positron are decay products of different hadrons inside jets. Di-jet production and fragmentation causes a correlation in the parent hadrons, which is inherited by the daughter electrons. When the electron and positron are from opposing (back-to-back) jets, the pair typically has low p_T and high mass. When they arise from two hadrons in the same jet, the pair typically has a high p_T and low mass.

Since cross pairs and jet pairs result from two e^+e^- pairs, correlated pairs with like and unlike-sign are produced at the same rate. This fact can be exploited to correct for correlated background in the unlike-sign distribution.

2. *Like-sign Subtraction*

The like-sign subtraction technique uses the foreground like-sign pairs $N_{\pm\pm}$ to determine the background. This has two distinct advantages over the event mixing technique. First, the measured yield $N_{\pm\pm}$ requires no additional absolute normalization. The second advantage, which was mentioned in the previous section, is that $N_{\pm\pm}$ contains the identical amount of correlated background as the measured e^+e^- pairs N_{+-}. Hence, no independent simulation of the correlated background is needed.

This method, however, can be used in PHENIX only after correcting for the different acceptance for like-sign and unlike-sign pairs of the two-arm configuration (see Fig. 1). This correction is provided by the ratio of the acceptance functions for unlike- and like-sign pairs, the relative acceptance correction, α, which is due solely to the detector geometry and is determined using mixed events as follows:

$$\alpha(m, p_T) = \frac{B^{\rm comb}_{+-}(m, p_T)}{B^{\rm comb}_{\pm\pm}(m, p_T)}. \qquad (6)$$

The ratio of mixed-event unlike-sign to like-sign pairs is calculated differentially in mass and p_T and is applied to each run group separately.

Figure 1 shows the mass distribution for the unlike and like-sign pairs in mixed events, $B^{\rm comb}_{+-}$and $B^{\rm comb}_{\pm\pm}$, respectively. Also shown is the mass spectrum for like-sign pairs $N_{\pm\pm}$. The relative acceptance correction translates $N_{\pm\pm}$to the unlike-sign pair space via $N_{+-} = \alpha \times N_{\pm\pm}$. Deviations between the α corrected like-sign spectrum and the unlike-sign mixed events correspond to the cross pairs and jet pairs.

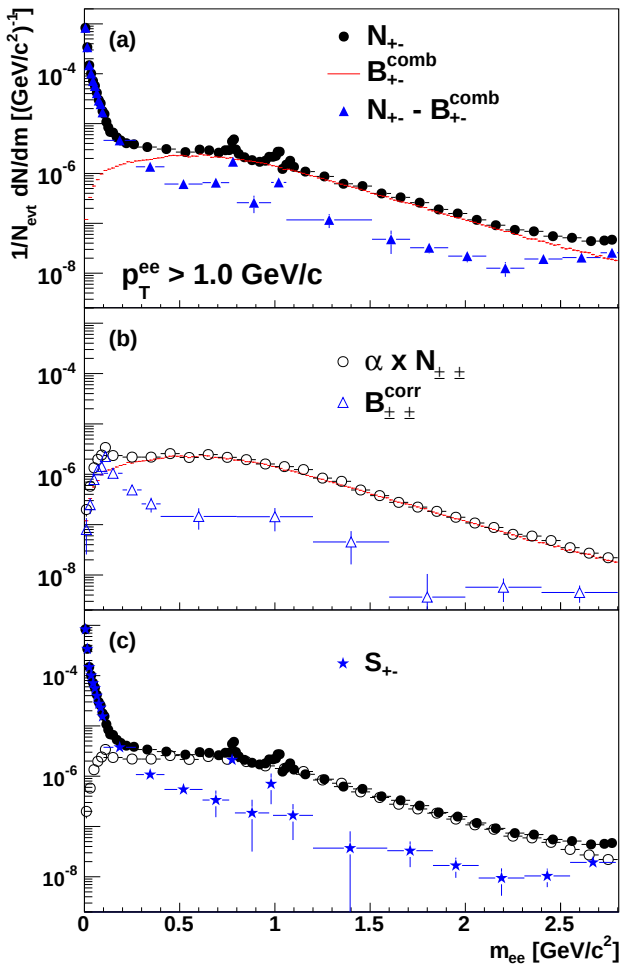

FIG. 2: The top panel shows the e^+e^- pair foreground N_{+-}, the combinatorial background $B^{\rm comb}_{+-}$ determined through event mixing, and the difference of the two which is the sum of the signal we are interested in S_{+-} and the correlated background $B^{\rm cor}_{+-}$ that still needs to be subtracted. Shown in the middle panel is the estimate of the correlated background $B^{\rm cor}_{+-}$, which is the difference between the foreground like-sign pairs $N_{\pm\pm}$ corrected for the relative acceptance difference α between $N_{\pm\pm}$and N_{+-}(see Fig. 1 and Eq. 6) and the combinatorial background $B^{\rm comb}_{+-}$. The bottom panel shows the signal S_{+-} which is calculated as $N_{+-} - \alpha \times N_{\pm\pm}$. In this plot, the combinatorial background is normalized in a region with minimal correlated background[22].

The subtraction procedure is illustrated in Fig. 2. It illustrates the steps to transform the measured e^+e^- pairs N_{+-}in Fig. 2(a) to the signal of interest S_{+-} in Fig. 2(c). Figure 2(a) shows N_{+-}, $B^{\rm comb}_{+-}$and their difference, which corresponds to the signal S_{+-}plus the correlated background $B^{\rm cor}_{+-}$. The middle panel of Fig. 2(b) shows $B^{\rm cor}_{+-}$ calculated as the difference, $\alpha \times N_{\pm\pm} - B^{\rm comb}_{+-}$. The signal S_{+-} is given in Fig. 2(c). The actual background subtraction is done double-differentially, and separately for each run group, as well as separately for minimum

bias and electron triggered events.

$$S_{+-}(m,p_T) = N_{+-}(m,p_T) - B^{\rm comb}_{+-} - B^{\rm cor}_{+-} \\ = N_{+-}(m,p_T) - \alpha(m,p_T) \times N_{\pm\pm}(m,p_T). \quad (7)$$

For the electron triggered events, the trigger used in the data collection biases the single electron distribution towards high p_T and as such the triggered events can not be mixed with each other. Thus to generate the correct combinatorial background shape of e^+e^- pairs, the mixed events are generated from the minimum bias data sample, but as in the real events, they are required to satisfy the trigger requirement. Every mixed pair therefore contains at least one electron that fulfills the trigger condition[26].

3. B meson decay chains

Approximately 1/3 of the ee pairs from $b\bar{b}$ production are like-sign pairs. Using the like-sign subtraction technique, these are removed from the signal S_{+-}. The main decay chains for B and D mesons to ee pairs are shown in Table. I. While for $c\bar{c}$, only the direct semi-leptonic decays, (1) in Table. I, contribute, many more possibilities exist for $b\bar{b}$. Decay combinations (1),(1) and (2),(2) lead to e^+e^- pairs, while combinations (2)(1) and (1)(2) lead to e^-e^- and e^+e^+ pairs due to the flavor change in the decay. The last decay chain (3) involves decay of a single b or $\bar{b}$ and produces only e^+e^- pairs. Since the semi-leptonic decay channels for B and D mesons have approximately equal branching ratios, and more than 90% of B mesons decay to D, all three groups of decays are approximately equally likely. This results in about a third of all ee pairs from $b\bar{b}$ decays being like-sign pairs.

TABLE I: Summary of the most relevant $c\bar{c}$ and $b\bar{b}$ decay chains that contribute to e^+e^- pairs. The effective branching ratio averages over all possible meson combinations.

Mode	Decay chain	Effective B.R.
(1)	$D \to e^+X$	9.4%
(1)	$B \to e^+X$	11%
(2)	$B \to \bar{D}X \to e^-X$	8.5%
(3)	$B \to \bar{D}e^+X \to e^+e^-X$	0.8%

Another important difference between ee pair production from $b\bar{b}$ compared to $c\bar{c}$ is that particle-antiparticle oscillations between B^0 and $\bar{B}^0$ can change one of the charges in an ee pair [27]. A B^0_d oscillates with a probability of ∼17% while a B^0_s does so ≈49% of the time [28]. Therefore, in the all decay chain combinations involving (1) or (2) from Table I, there is 20% probability for a sign change.

It is thus vital to treat the simulations with the same procedure as the data in order to properly account for all of the heavy flavor pairs. Both PYTHIA [29] and Monte Carlo at next-to-leading-order (MC@NLO) [30] calculations generate the proper like-sign yield from heavy flavor sources. As in the data analysis, we subtract this like-sign contribution from the unlike-sign yield in the simulations. Only then are comparisons made to the data.

C. Efficiency Corrections

The e^+e^- signal S_{+-} is corrected for single particle detection and identification efficiency to obtain the di-electron yield in the PHENIX acceptance:

$$\frac{d^2N}{dm_{ee}dp_T^{ee}} = \frac{1}{N_{\rm evt}^{sampled}} \cdot \frac{1}{\Delta m_{ee}} \cdot \frac{1}{\Delta p_T^{ee}} \cdot \frac{1}{\varepsilon_{\rm rec}(m,p_T)} \cdot \frac{1}{\varepsilon_{\rm ERT}(m,p_T)} \cdot S_{+-}(m,p_T) \cdot C_{\rm bias}. \quad (8)$$

The reconstruction efficiency $\varepsilon_{\rm rec}(m,p_T)$ is evaluated using a GEANT3Monte Carlo simulation of the PHENIX detector. It accounts for losses in yield due to dead areas in the detector, track reconstruction efficiency, single track quality cuts, electron identification cuts, and e^+e^- pair cuts. Since the detector performance varies from run group to run group, efficiency is evaluated separately for each run group. The inverse $(\varepsilon_{\rm rec}(m,p_T))^{-1}$ is used to correct the S_{+-} to represent the yield in the ideal PHENIX acceptance[1]. No correction is made for pair acceptance, as the magnitude of such corrections depends upon the pair production process and thus the opening angle between the electron and positron.

The trigger efficiency $\varepsilon_{\rm ERT}(m,p_T)$ for e^+e^- pairs is measured by requiring that one of the electrons in the pair satisfies the single electron trigger conditions. The resulting mass spectrum is compared to that from minimum bias events to evaluate the trigger efficiency. The trigger approaches full efficiency for pair masses above approximately 2 GeV/c^2.

The factor $C_{\rm bias} = 0.889 \pm 0.003$ accounts for the correlation between heavy flavor events and an increase in the charge deposited in the BBC [24] as well as any inefficiency in the BBC trigger. It is calculated in a Glauber Monte Carlo-based framework that includes the BBC response. The corrected yield represents the heavy flavor yield corresponding to the inelastic d+Au cross section of $\sigma^{d\rm Au}_{\rm inel} = 2.3 \pm 0.1$ b [24].

[1] The PHENIX acceptance is parameterized as function of the azimuthal angle ϕ of a track, its p_T, and charge sign q by conditions for the DC and the RICH for each spectrometer arm separately: $\phi_{\rm min} < \phi + qk_{\rm DC}/p_T < \phi_{\rm max}$ and $\phi_{\rm min} < \phi + qk_{\rm RICH}/p_T < \phi_{\rm max}$. The parameters are $k_{\rm DC} = 0.206$ rad GeV/c, $k_{\rm RICH} = 0.309$ rad GeV/c, $\phi_{\rm min} = -3/16\pi$ to $\phi_{\rm max} = 5/16\pi$, and$\phi_{\rm min} = 11/16\pi$ to $\phi_{\rm max} = 19/16\pi$.

D. Systematic Uncertainties

The systematic uncertainties on the e^+e^- yield arise from uncertainties on the dielectron reconstruction efficiency, the single electron trigger efficiency, and the precision of the background determination.

The uncertainty on electron reconstruction is based on the reproducibility of the final result using multiple cut variations both on single electrons and on electron pairs. The cuts varied include electron identification, conversion rejection, and pair cuts. The conversion rejection and pair cuts are less influential and only affect the low mass region ($<$ 600 MeV/c^2). The uncertainties are evaluated by reconstructing simulated dielectrons using a full GEANT3 Monte Carlo simulation of the PHENIX detector. Detector dead areas can vary slightly within a given performance-based run group. Typical run-by-run variations were analyzed in addition to group-by-group variations, in order to evaluate the systematic uncertainties from detector performance. In the intermediate (1-3 GeV/c^2) and high mass regions (>3 GeV/c^2), these uncertainties vary between 10-20%.

The precision of the trigger efficiency correction depends on the available statistics in the minimum bias data sample as well as on the super module segmentation of the EMCal. An EMCal super module is a group of 12$\times$ 12 (or 6 $\times$ 4) lead-scintillator towers[31]. The trigger efficiency is calculated using the statistically independent minimum bias data for each EMCal super module separately within each run group. The single electron trigger efficiencies are then used in the simulation to obtain pair trigger efficiency. The triggered data is used above pair $m_T > 1.5$ GeV/c and contributes only a 5% uncertainty to the final result.

The dominant source of systematic uncertainty is the accuracy of the relative acceptance correction. Since it is a mass and p_T dependent scale factor applied directly to the background, it affects the overall uncertainty in proportion to the background-to-signal ratio. This correction is very sensitive to the fluctuations in detector dead area that exist within a run group. Dedicated Monte Carlo simulations were performed to determine the effect of removing or including various regions of the PHENIX central arms. These regions were chosen to reflect realistic geometry including EMCal modules/super modules, DC wires grouped by power input and signal output, and shifted positions of intrusive support structures. This uncertainty ranges from <5% at high mass (>5 GeV/c^2) to $\sim$25% below 2.5 GeV/c^2.

Table II summarizes the magnitude of the systematic uncertainty arising from various sources and the affected mass ranges.

TABLE II: Systematic uncertainties of the dilepton yield due to different sources with an indication of the applicable mass range. The transverse mass is defined as $m_T = \sqrt{m^2 + p_T^2}$.

Component	Syst.uncertainty	Mass (GeV/c^2)
Pair reconstruction	14%	0–14
Conversion rejection	6%	0–0.6
	0%	>0.6
Pair cuts	5%	0.4–0.6
Trigger efficiency	5%	$m_T \geq 1.5$
Dead area, run groups	15%	0–2.5
	10%	2.5–14
Relative acceptance	5%$\times B/S$	0–2.5
	2%$\times B/S$	2.5–5
	1%$\times B/S$	>5

IV. RESULTS

A. Yield of e^+e^- pairs

Figure 3 shows the mass projection of the measured double differential e^+e^- pair yield in the ideal PHENIX acceptance (as described in footnote[1]). The inset shows the mass spectrum up to 4.5 GeV/c^2, and a detailed cocktail of hadronic decay sources that contribute to the mass spectrum below 4.5 GeV/c^2. The main figure shows the mass distributions of charm, bottom and Drell-Yan e^+e^- pairs obtained using PYTHIA. One can clearly see that the resonances lie atop a continuum, which is dominated by three body decays of pseudoscalar and vector mesons for masses below 1.0 GeV/c^2. Above 1.0 GeV/c^2 the continuum is dominated by pairs from semi-leptonic decays of heavy flavor, with the bottom contribution becoming more important at higher mass.

The lower panel of the Figure 3 shows the ratio of data to the expected sources. The shape of the measured mass spectrum is well described by the expected sources over the entire mass range. For the mass range below 1.0 GeV/c^2, the cocktail is absolutely normalized and shows a good agreement to the data. For the high mass region, the e^+e^- pair continuum from heavy flavor decays is normalized to the data to extract the bottom and charm cross section as discussed below.

B. Expected sources of e^+e^- pairs

Many sources contribute to the inclusive e^+e^- pair yield, so an in-depth understanding of the expected sources and their double differential distribution in e^+e^- pair mass and p_T is necessary to interpret the data. We use the detailed component-by-component simulation developed in [25], as a benchmark. The cocktail includes pseudoscalar and vector meson decays, semi-leptonic decays of heavy flavor, and e^+e^- pairs created through the

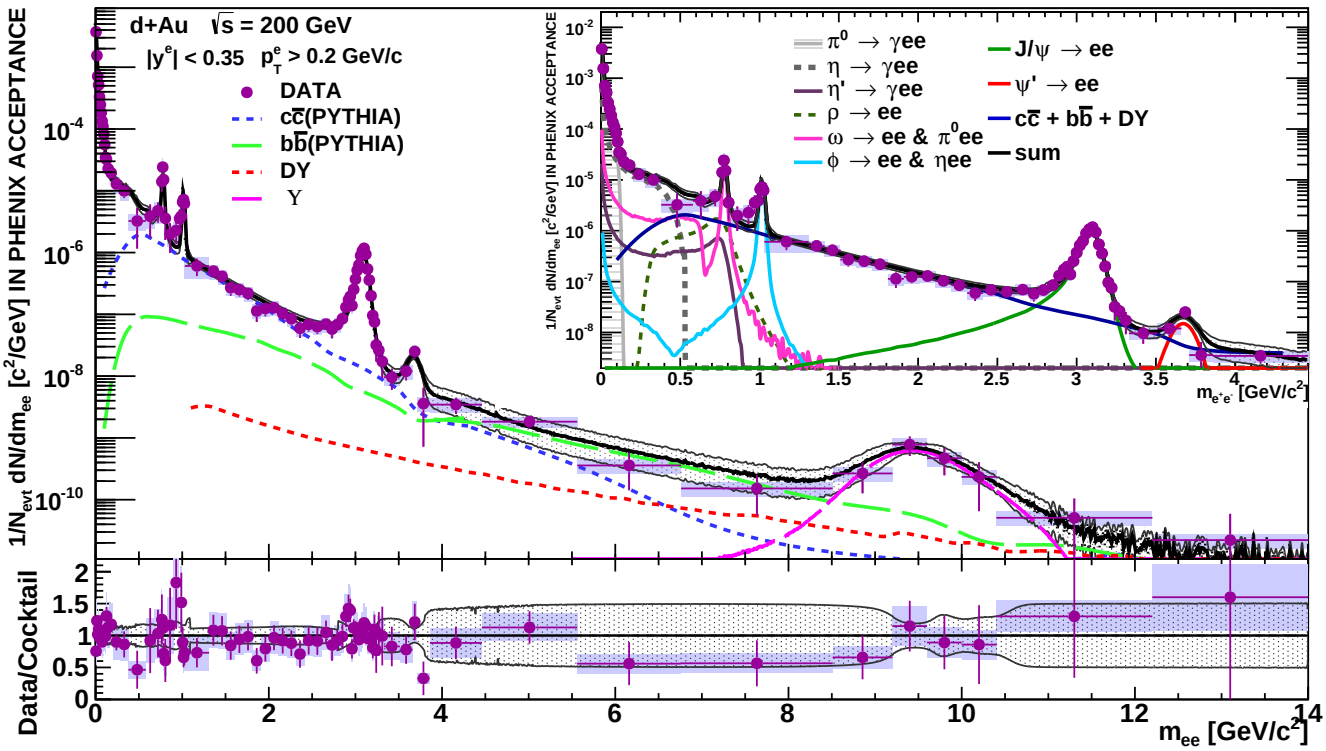

FIG. 3: Inclusive e^+e^- pair yield from minimum bias d+Au collisions as a function of mass. The data are compared to our model of expected sources. The inset shows in detail the mass range up to 4.5 GeV/c^2. In the lower panel, the ratio of data to expected sources is shown with systematic uncertainties.

Drell-Yan mechanism.

The pseudoscalar mesons, π^0 and η, and vector mesons, ω, ϕ, J/ψ and the Υ, are generated based on measured differential d+Au cross sections [32–37]. The contributions from mesons not directly measured in d+Au (η', ρ, and ψ') are determined relative to the measured mesons (η, ω, J/ψ, respectively) using particle ratios from p+p or jet fragmentation [22]. Decay kinematics, branching ratios, electromagnetic transition form factors, etc. are based on the most up-to-date information from the Particle Data Group [38]. The yield of e^+e^- pairs created through the Drell-Yan mechanism was simulated using PYTHIA[2] For the normalization we use a cross section of 34 ± 28 nb, which was determined by a simultaneous fit of the data at high mass to Drell-Yan, charm, and bottom contributions using the PYTHIAsimulation. The systematic uncertainty in the Drell-Yan cross section is propagated through the subsequent heavy flavor cross section analysis. This uncertainty has a negligible effect ($< 5\%$) on the final result of the bottom cross section. As can be seen from Fig. 3, the contribution from Drell-Yan is extremely small below ≈ 5 GeV/c^2. It remains a minor contribution to the dielectron pair spectrum below 10 GeV/c^2.

The double differential contribution from semi-leptonic decays of heavy flavor are simulated using two different p+p event generators, PYTHIAand MC@NLO. The cross sections for $c\bar{c}$ and $b\bar{b}$ in the cocktail shown in Fig. 3 are the ones extracted from this work, as discussed below.

The PYTHIAprogram generates heavy quark pairs by calculating the leading order pQCD gluon fusion contributions. We used PYTHIAin forced $c\bar{c}$ or $b\bar{b}$ production mode[3] to match Ref. [22], and CTEQ5L as the input parton distribution function.

The MC@NLOpackage (v. 4.03) [30, 39] is an NLO simulation that generates hard scattering events to be passed to HERWIG(vers. 6.520) [40] for fragmentation into the vacuum. Since the package is a two-step procedure consisting of event generation and then fragmentation, care is taken to pass the color flow of each parton configuration from the generator to HERWIG. In addition, since flavor creation (i.e., $qq \to QQ$ and $gg \to QQ$) processes

[2] Drell-Yan PYTHIA-6 [29], using parameters: MSEL=0, MSTP(43)=3, MSTP(33)=1, MSTP(32)=1, MSUB(1)=1, MSTP(52)=2, MSTP(54)=2, MSTP(56)=2, MSTP(51)=10041 (CTEQ6LL), MSTP(91)=1, PARP(91)=1.5, MSTP(33)=1, MSTP(31)=1.38, MSTP(32)=4, CKIN(3)=0.5, CKIN(1)=0.5, CKIN(2)=-1.0, CKIN(4)=-1.0, MSTP(71)=0

[3] Heavy flavor PYTHIA-6 [29], using parameters MSEL=4 ($c\bar{c}$) or 5 ($b\bar{b}$), MSTP(91)=1, PARP(91)=1.5, MSTP(33)=1, PARP(31)=1.0, MSTP(32)=4, PMAS(4)=1.25, PMAS(5)=4.1”

at order α_S^2 can generate some of the higher order processes through parton showering, MC@NLOkeeps track of this to ensure an accurate result. While the default MC@NLOpackage generates $b\bar{b}$ events, it does not incorporate $c\bar{c}$ events. Thus, we altered the default package to enable charm production[4]. Because both MC@NLOand HERWIGuse the standard PDG process ID codes [38], we changed the process code from -1705 ($H_1H_2 \to b\bar{b} + X$) to -1704 ($H_1H_2 \to c\bar{c}+X$) and adjusted the heavy quark mass to the charm quark, 1.29 GeV/c^2. No other parameters were modified. In contrast to PYTHIA, the running parameters of MC@NLOdoes not need to be fine-tuned for different analyses. CTEQ6M [41] was used to provide the input parton distribution function.

The electrons and positrons from all simulations are filtered through the PHENIX acceptance [25]. The e^+e^- pair acceptance depends on the production process, which determines the correlation between the electron and positron. For pseudoscalar and vector meson decays, the e^+e^- pairs originate from an intermediate virtual photon that correlates the momenta of e^+ and e^-. For e^+e^- pairs from heavy flavor decays the correlation is governed by the interplay of two contributions: (i) the QCD production of the $q\bar{q}$ pair, which determines the rapidity distribution of the pair, the rapidity gap between q and $\bar{q}$ and the extent to which they are back-to-back in azimuthal angle; and (ii) the decay kinematics of the two independent semi-leptonic decays. The latter tends to randomize the correlation if the mass of the quark is large compared to its momentum. In the limit of very large quark masses the decays will occur at rest and the e^+ and e^- momenta will be determined exclusively by the independent decays. In contrast, for small quark masses the decay products will be boosted along the momenta of the parent quarks and thus their correlation will closely reflect the correlations between the parent quarks.

The differences between the acceptance for e^+e^- pairs from charm and bottom production are documented in Tables III to VI. While only 1 out of 500 e^+e^- pairs from charm production is accepted in PHENIX, 1 out of 120 pairs from bottom production is accepted. This can be compared to the limiting case of very large quark masses, for which the direction of the decay e^+ and e^- are independent and approximately 1 of 80 e^+e^- pairs will fall into the PHENIX acceptance. The acceptance for e^+e^- pairs from $b\bar{b}$ is only 30% different from this limiting case, while for $c\bar{c}$ the deviation is more than a factor of five. This suggests that the acceptance for pairs from $b\bar{b}$ is driven mostly by decay kinematics, and thus depends only a little on the correlation between the b and $\bar{b}$. Consequently the model dependence must be much smaller for $b\bar{b}$ than for $c\bar{c}$.

Comparing PYTHIAand MC@NLOin Table IV and Table VI shows that indeed the difference between the acceptance calculated with PYTHIAand MC@NLOis much smaller for $b\bar{b}$ than for $c\bar{c}$ pairs. For bottom production the difference is about 5%, while in the charm case the acceptance is different by a factor of 1.2, which increases to 2.2, if one restricts the mass range to above 1.16 GeV/c^2. Most of this model-dependence is already apparent when going from 4π to a restricted rapidity coverage of $\Delta y = 1$ for e^+ and e^-, and does not significantly increase when restricting to the smaller PHENIX aperture.

The correlations of the q and $\bar{q}$ are very different in PYTHIAand MC@NLO. While in MC@NLOthe correlation is due to including NLO terms explicitly in the pQCD calculation, in the first order PYTHIAcalculation the correlation is largely determined by the specific implementation of intrinsic transverse momentum (k_T). While both models predict similar momentum distributions for the indi-

TABLE III: Number of $c\bar{c}$ pairs at midrapidity in $y_{c\bar{c}} = 1$ and $y_{c\bar{c}} = 0.7$ relative to 4π. $y_{c\bar{c}}$ corresponds to the rapidity of center-of-mass of $c\bar{c}$ pair.

Acceptance	PYTHIA$c\bar{c}$ pairs	MC@NLO$c\bar{c}$ pairs
4π	1	1
$\lvert y_{c\bar{c}}\rvert < 0.5$	0.275	0.297
$\lvert y_{c\bar{c}}\rvert < 0.35$	0.2	0.215

TABLE IV: Yields of e^+e^- pairs from $c\bar{c}$, measured in units of one $c\bar{c}$ pair per event divided by the effective semi-leptonic branching ratio squared $F_{BR}^{c\bar{c}} = (B.R.(c \to e))^2$, where B.R. is the effective branching ratio of 9.4%.

Acceptance	PYTHIAe^+e^- pairs from $c\bar{c}$ [$F_{BR}^{c\bar{c}\,-1}$]	MC@NLOe^+e^- pairs from $c\bar{c}$ [$F_{BR}^{c\bar{c}\,-1}$]
4π	1	1
$\lvert y_{e^+}\&y_{e^-}\rvert < 0.5$	0.042	0.035
$\lvert y_{e^+}\&y_{e^-}\rvert < 0.5$ && $m_{e^+e^-} > 1.16$GeV/c^2	0.0047	0.00022
$\lvert y_{e^+}\&y_{e^-}\rvert < 0.35$	0.021	0.017
$\lvert y_{e^+}\&y_{e^-}\rvert_{\text{PHENIX}}$	0.0023	0.0016
$\lvert y_{e^+}\&y_{e^-}\rvert_{\text{PHENIX}}$ && $m_{e^+e^-} > 1.16$GeV/c^2	0.00044	0.0002

TABLE V: Number of $b\bar{b}$ pairs at midrapidity in $y_{b\bar{b}} = 1$ and $y_{b\bar{b}} = 0.7$ relative to 4π. $y_{b\bar{b}}$ corresponds to the rapidity of center-of-mass of $b\bar{b}$ pair.

Acceptance	PYTHIA$b\bar{b}$ pairs	MC@NLO $b\bar{b}$ pairs
4π	1	1
$\lvert y_{b\bar{b}}\rvert < 0.5$	0.39	0.40
$\lvert y_{b\bar{b}}\rvert < 0.35$	0.28	0.29

[4] This trivial adaptation was reviewed by the original MC@NLOauthors via private communication.

TABLE VI: Yields of e^+e^- pairs from $b\bar{b}$, measured in units of one $b\bar{b}$ pair per event divided by the effective semi-leptonic branching ratio squared $F_{BR}^{b\bar{b}} = (B.R.(b \to e))^2$, where B.R. is the effective branching ratio of 15.8% using a like-sign pair subtraction, or 22% not considering the like-sign pairs.

Acceptance	PYTHIA e^+e^- pairs from $b\bar{b}$ $[F_{BR}^{b\bar{b}\,-1}]$	MC@NLO e^+e^- pairs from $b\bar{b}$ $[F_{BR}^{b\bar{b}\,-1}]$
4π	1	1
$\lvert y_{e^+}\&y_{e^-}\rvert < 0.5$	0.095	0.091
$\lvert y_{e^+}\&y_{e^-}\rvert < 0.5$ $m_{e^+e^-} > 1.16\mathrm{GeV}/c^2$	0.0425	0.0395
$\lvert y_{e^+}\&y_{e^-}\rvert < 0.35$	0.048	0.046
$\lvert y_{e^+}\&y_{e^-}\rvert_{\mathrm{PHENIX}}$	0.0084	0.0080
$\lvert y_{e^+}\&y_{e^-}\rvert_{\mathrm{PHENIX}}$ $m_{e^+e^-} > 1.16\mathrm{GeV}/c^2$	0.00368	0.0037

vidual q and $\bar{q}$, the opening angle distributions for the $q\bar{q}$ pairs are different and thus the mass distributions in 4π differ substantially. These differences decrease upon selecting decay e^+e^- pairs that fall in the PHENIX acceptance, so the shape of the mass and p_T distributions from the two models are quite similar. Thus in the PHENIX acceptance, the model differences in the $q\bar{q}$ correlations surface mostly through different fractions of e^+e^- pairs that fall in the acceptance.

For $b\bar{b}$ pairs the decay kinematics have a different effect than for $c\bar{c}$. About 50% of the e^+e^- pairs from $b\bar{b}$ production involve only the decay of the b or $\bar{b}$ quark through the decay chain (3) from Table I and thus are *a priori* insensitive to the opening angle of the $b\bar{b}$ pair.

Since more than 90% of the B-mesons have momenta much smaller than their mass, the decay electron is less likely to move in the same direction as the parent meson. Consequently the correlation between e^+ and e^- from decays of b *and* $\bar{b}$ through decay chains (1) and (2) in Table I is smeared. The fraction of e^+e^- pairs in our acceptance from $b\bar{b}$ is much less sensitive to the correlations between the b and $\bar{b}$. We have tested this conclusion by randomizing the correlation between b and $\bar{b}$ and found that the acceptance remains unchanged while there is a significant difference for $c\bar{c}$.

Since the acceptance of e^+e^- pairs from $b\bar{b}$ is mostly driven by decay kinematics and not by the model dependent production mechanism, the fraction of e^+e^- pairs must also be less sensitive to any cold-nuclear-matter effects that alter the b or $\bar{b}$ after they are produced. For the lighter $c\bar{c}$ quarks the sensitivity to the opening angle between the c and $\bar{c}$ is much larger, implying larger model dependence and consequently cold-nuclear-matter effects may have a larger influence on the distribution of dielectrons from $c\bar{c}$. The results obtained in this analysis seem also insensitive to nuclear modifications of the parton distribution function; when using EPS09 [42] for the MC@NLO or PYTHIA calculation the acceptance factor for e^+e^- pairs from $b\bar{b}$ and $c\bar{c}$ production change by less than 5%.

The simulated e^+e^- pairs are folded with the experimental momentum resolution as well as with the energy loss due to bremsstrahlung. As a result we obtain the double differential e^+e^- pair yield for the expected sources that can be directly compared to the measured yield. All components are absolutely normalized, except for the heavy flavor contributions, which are used to determine the bottom and charm cross section from the e^+e^- pair data, and the Drell-Yan contribution, which is negligibly small and was fixed to be consistent with the data.

C. e^+e^- pairs from heavy flavor decays

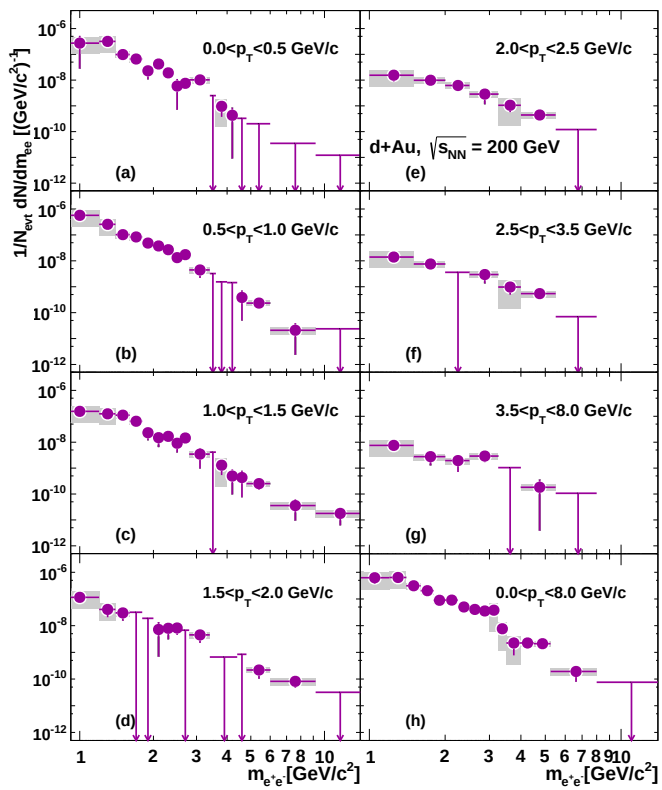

FIG. 4: Double differential e^+e^- pair yield from semi-leptonic decays of heavy flavor in inelastic d+Au collisions. Shown are mass projections in slices of p_T. The p_T intervals are indicated in each panel. Systematic uncertainties are shown as bars, downward pointing arrows indicate upper limits at 90% CL.

In order to access the heavy flavor yield, we subtract the yield of the pseudoscalar and vector mesons as well as the Drell-Yan contribution from the measured dielectron spectra. The subtraction is done double differentially in mass and p_T. The results are shown in Fig. 4 as mass spectra in slices of transverse momentum. The

data are plotted above 1.0 GeV/c^2, as lower mass e^+e^- are dominated by hadronic decay contributions. In the mass regions where the inclusive e^+e^- yield is dominated by vector meson decays only upper limits can be quoted for the subtracted spectra. We use p_T bins of 500 MeV/c up to p_T =3 GeV/c. Above p_T = 3.0 GeV/c, statistical limitations dictate the use of broader p_T bins.

V. HEAVY FLAVOR CROSS SECTION DETERMINATION

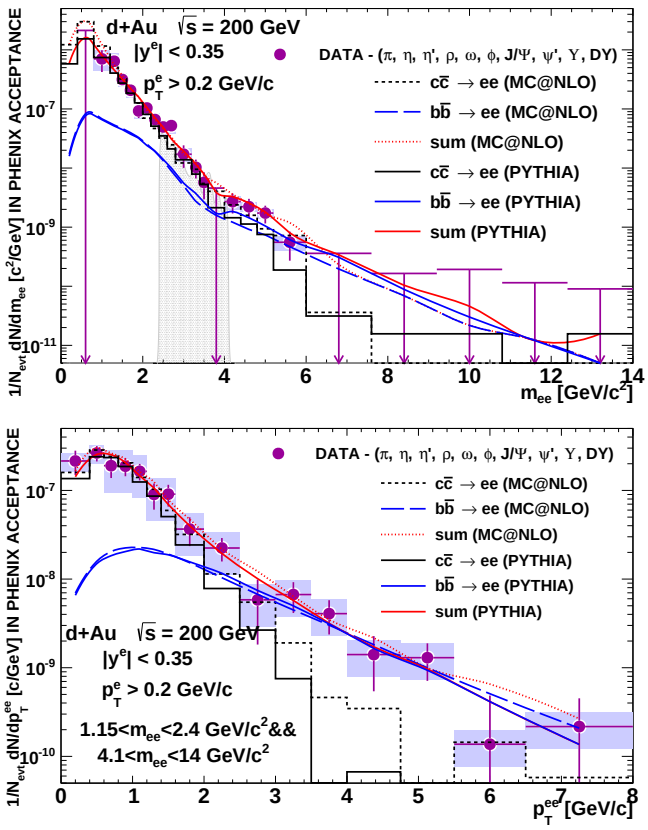

FIG. 5: Top panel compares the mass dependence of e^+e^- pair yield with PYTHIAand MC@NLOcalculations. The bottom panel shows the comparison for the p_T dependence. The gray panel shown in top panel is not used in the fitting and is excluded in the p_T projection.

Figure 5 compares the projections of the e^+e^- yield from heavy flavor decays onto the mass and p_T axes to the PYTHIAand MC@NLOcalculations. The absolute normalization of each calculation was adjusted to the data as discussed below. The shape of the measured distributions is well described by both simulations. Both projections illustrate the fact that bottom production is dominant at high mass or p_T.

In the double differential spectra, the separation of e^+e^- pairs from charm and bottom decays becomes even more evident. This is illustrated in Fig. 6. At lower pair

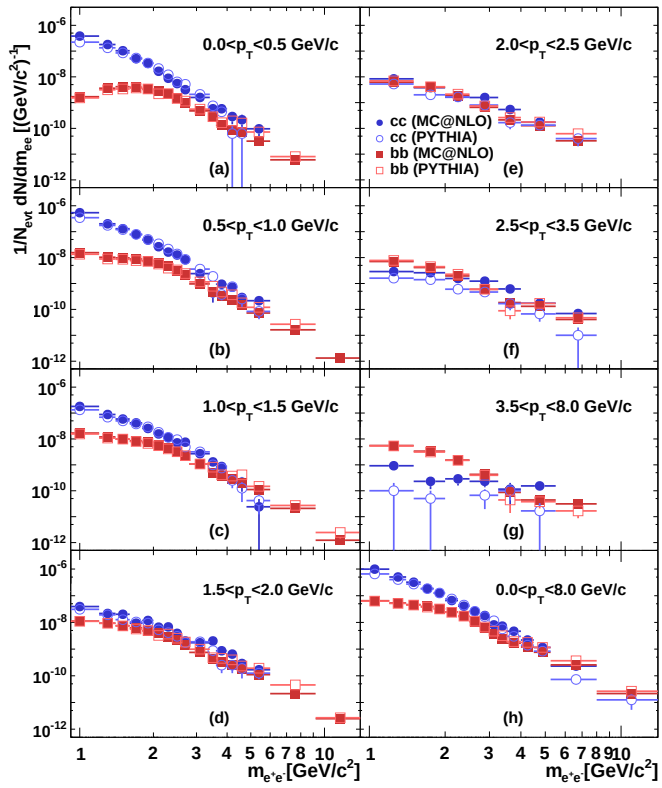

FIG. 6: Double differential e^+e^- pair yield from semi-leptonic decays of heavy flavor as simulated by PYTHIAand MC@NLO. Shown are mass projections in slices of p_T. The p_T intervals are indicated in each panel.

momenta, charm production dominates the yield below 3 GeV/c^2 mass. This dominance vanishes around $p_T = 2$ GeV/c and reverses at higher p_T, where bottom production dominates. Note that this separation of bottom and charm in mass versus p_T is predicted by both generators and is thus model independent.

To separate bottom and charm yields quantitatively, we fit the distributions shown in Fig. 6 to the data shown in Fig. 4 with two free parameters, $N_{c\bar{c}}$ and $N_{b\bar{b}}$. These, in turn, are used to determine the charm and bottom cross sections.

The fits are performed according to

$$\frac{dn_{ee}^{hf}}{dmdp_T}\Big|_{\text{PHENIX}} = N_{c\bar{c}}\frac{dn_{ee}^{c\bar{c}}}{dmdp_T} + N_{b\bar{b}}\frac{dn_{ee}^{b\bar{b}}}{dmdp_T}, \qquad (9)$$

where the left hand side is the measured yield per minimum bias triggered event, as shown in Fig. 4. The $n_{ee}^{c\bar{c}}$ and $n_{ee}^{b\bar{b}}$ are determined either using the PYTHIAsimulation or the MC@NLOsimulation, where the simulation output was normalized to one $c\bar{c}$ or $b\bar{b}$ pair in 4π. The n_{ee} include the branching ratios for both the quark and anti-quark to decay semi-leptonically. Furthermore, the simulated spectra require that the decay e^+ and e^- each have $p_T > 200$ MeV/c and that both fall into the PHENIX acceptance and satisfy an explicit cut on the pair $m_T > 450$ MeV/c. The fits are per-

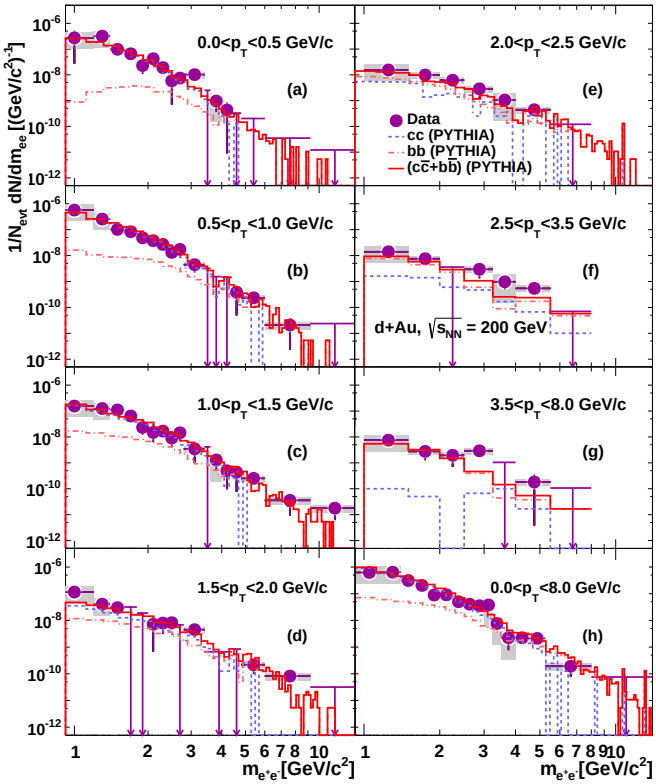

FIG. 7: Double differential e^+e^- pair yield from heavy flavor decays fitted to simulated distributions from PYTHIA. The mass region highlighted by the gray band in Fig. 5 is excluded from the fitting.

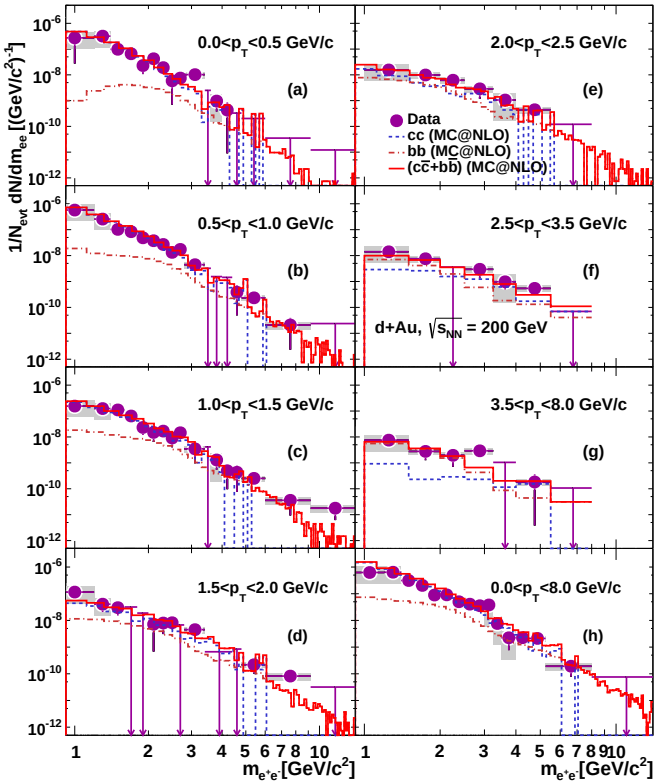

FIG. 8: Double differential e^+e^- pair yield from heavy flavor decays fitted to simulated distributions from MC@NLO. The mass region highlighted by the gray band in Fig. 5 is excluded from the fitting.

formed in the mass range $1.15 < m_{e^+e^-} < 2.4$ GeV/c^2 and $4.1 < m_{e^+e^-} < 14$ GeV/c^2, for both data and simulations. In this normalization scheme, the fit parameters $N_{c\bar{c}}$ and $N_{b\bar{b}}$ are equal to the average number $c\bar{c}$ pairs and of $b\bar{b}$ pairs per inelastic d+Au event.

The fit results are shown in Fig. 7 and Fig. 8 using the PYTHIAand MC@NLOdistributions, respectively. The resulting χ^2 per degree of freedom (NDF) is 147/81 for PYTHIAand 162/81 for MC@NLO. This χ^2 is calculated using statistical uncertainty on the data points only. If we add the systematic uncertainties in quadrature with the systematic uncertainties, the χ^2/NDF is 30/81 and 34/81 for PYTHIAand MC@NLO, respectively. These χ^2/NDF represent extremes because the statistical uncertainty ignores the uncorrelated systematic uncertainty while including the total systematic uncertainty incorrectly includes correlated uncertainties. Because we do not know the fraction of the correlated and uncorrelated systematic uncertainty in the total quoted systematic uncertainty, we conservatively assume that it is entirely correlated and use the fit results from the corresponding case.

For the PYTHIAsimulation we obtain the fit parameters:

$$N_{c\bar{c}} = 0.069\pm0.006(\text{stat})\pm0.021(\text{syst}) \quad (10)$$
$$N_{b\bar{b}} = 0.00061\pm0.00011(\text{stat})\pm0.00019(\text{syst}) \quad (11)$$

and for the MC@NLO

$$N_{c\bar{c}} = 0.172\pm0.017(\text{stat})\pm0.060(\text{syst}) \quad (12)$$
$$N_{b\bar{b}} = 0.00060\pm0.00014(\text{stat})\pm0.00020(\text{syst}) \quad (13)$$

The quoted systematic uncertainties were determined by refitting the data points varied up, then down, by one σ_{syst}.

Additional systematic uncertainties arise from the models themselves. In the MC@NLOcalculation model uncertainties were evaluated by varying the renormalization scale by a factor of 2 up and down; the uncertainties are found to be 5% and 2.5% for charm and bottom respectively. These are quadratically small compared to those arising from the data uncertainties. For PYTHIAno separate evaluation of scale-dependence was done.

A second type of model-dependence in the cross section arises from the dependence of the pair acceptance on the quark-antiquark correlation from the QCD production process, as discussed above. By comparing results obtained with the different simulations we can see that the model dependence of the bottom cross sections are less than 2%. For charm production, on the other hand, the extracted cross sections differ by 50% . The large difference in the model dependence of the extracted charm and bottom cross sections results from the fact that the bottom mass is much larger and thus the fraction of e^+e^-

TABLE VII: Compilation of the published $b\bar{b}$ cross sections.

$\sigma_{bb}(\mu\text{b})$	Reference
3.4±0.8 (stat)±1.1 (syst)	This work
$3.2^{+1.2}_{-1.1}$ (stat)$^{+1.4}_{-1.3}$ (syst)	[20]
3.9 ± 2.5 (stat)$^{+3}_{-2}$ (syst)	[22]
4.0 ±0.5 (stat) ± 1.1 (syst)	[14]

pairs that fall into the PHENIX acceptance is dominated by the decay kinematics. For charm production the correlation between c and $\bar{c}$ contribute more significantly.

With the fit parameter $N_{b\bar{b}}$ from above, and the acceptance relations in Table V, we can determine rapidity densities and cross sections for bottom production in d+Au collisions. The cross section follows as:

$$\sigma_{b\bar{b}}^{d\text{Au}} = N_{b\bar{b}} \times \sigma_{\text{inel}}^{d\text{Au}} \tag{14}$$

We find 1.38 μb and 1.36 μb using the $N_{b\bar{b}}$ determined using PYTHIAor MC@NLO, respectively; there is essentially no model dependence in the extracted cross sections. Consequently, we report the bottom production cross section of:

$$\sigma_{b\bar{b}}^{d\text{Au}} = 1.37\pm0.28(\text{stat})\pm0.46(\text{syst})\text{mb} \tag{15}$$

and a corresponding rapidity density at midrapidity averaged over $\Delta y = 1$ of:

$$\left.\frac{d\sigma_{b\bar{b}}^{d\text{Au}}}{dy}\right|_{y=0} = 0.54\pm0.11(\text{stat})\pm0.18(\text{syst})\text{mb} \tag{16}$$

The average number of binary collisions is 7.6 ± 0.4 in inelastic d+Au events[24], and the inelastic p+p cross section is $\sigma_{\text{inel}}^{pp} = 42 \pm 3$ mb. The quoted systematic uncertainty on the cross section includes all uncertainties, but is dominated by those on the measurement itself.

This is the first measurement of the $b\bar{b}$ cross section in d+Au collisions. One can naively extract a nucleon-nucleon equivalent $b\bar{b}$ cross section, and find it to be $\sigma_{bb}^{NN} = 3.4\pm0.8(\text{stat})\pm1.1(\text{syst})$ μb. This value is consistent with the other $b\bar{b}$ cross section values as reported by other measurements, and a comparison is shown in the Table. VII.

Cold-nuclear-matter effects have been measured for heavy flavor in d+Au [13, 17–19]. In some cases, the effects are small enough to be within the quoted uncertainties of the measurement presented here. In others, they occur at forward or backward rapidity where the effects will not be observed by these data at midrapidity.

The determination of the charm cross section is less reliable due to the large model dependence. Using the PYTHIAcalculation we find $\sigma_{c\bar{c}}^{pp} = 385\pm34(\text{stat})\pm119(\text{syst})$ μb and for the MC@NLOcalculation we find $\sigma_{c\bar{c}}^{pp} = 958\pm96(\text{stat})\pm335(\text{syst})$ μb. We conclude that the large model dependence does not allow an accurate determination of the charm cross section from our e^+e^- pair measurement. As shown in Table IV, the model dependence of the pair acceptance is already substantial for detection of pairs with mass > 1.16 GeV/c^2 in one unit of rapidity. To test predictions for cold-nuclear-matter effects with dilepton data will require comparisons within specific models. Calculations should compare the shape of the predicted e^+e^- mass and p_T spectra to those presented in Fig. 4 and Fig. 5.

VI. SUMMARY AND CONCLUSIONS

PHENIX recorded a large sample of e^+e^- pairs from d+Au collisions at $\sqrt{s_{_{NN}}} = 200$ GeV in 2008. The e^+e^- pair yield is consistent with the expected yield from pseudoscalar and vector meson decays and semi-leptonic decays of heavy mesons. The high statistical precision of the data allows exploration of both the mass and p_T dependence of the e^+e^- yield. Using the double differential information, we can clearly isolate the contribution of heavy flavor decays and determine the fraction of the yield from $c\bar{c}$ and $b\bar{b}$ production. We report the first measurement of the $b\bar{b}$ production cross section in d+Au collisions.

Our procedure utilizes model predictions of the shape of the double differential e^+e^- spectra from $b\bar{b}$ and $c\bar{c}$ production, with a filter requiring that the e^+ and e^- fall inside the PHENIX central arm acceptance. The two simulations used in this work, PYTHIAand MC@NLO, predict very different correlations between the q and $\bar{q}$. In PYTHIAthe $q\bar{q}$ correlation is driven by the particular implementation of intrinsic k_T, while in MC@NLOthe $q\bar{q}$ correlation arises from including NLO terms in the calculation.

For $b\bar{b}$ production, the fraction of e^+e^- pairs at midrapidity, and therefore also in the PHENIX acceptance, is primarily determined by the decay kinematics of the two independent semi-leptonic decays and is not sensitive to the substantial model dependence on the $b\bar{b}$ correlations. For the same reason, the fraction of e^+e^- pairs at midrapidity is not sensitive to possible modifications of the momenta for b and $\bar{b}$ due to cold-nuclear-matter effects. Determination of the $b\bar{b}$ cross section thus has little model dependence and the measured e^+e^- double differential spectra can be used to reliably calculate the production cross section, for which we find:

$$\sigma_{b\bar{b}}^{d\text{Au}} = 1.37\pm0.28(\text{stat})\pm0.46(\text{syst})\ \text{mb}, \tag{17}$$

A search for cold-nuclear-matter effects will be possible by comparing the double differential results reported here with those in p+p collisions. The current result should already help to constrain models of cold-nuclear-matter effects on heavy quark production.

ACKNOWLEDGMENTS

We thank the staff of the Collider-Accelerator and Physics Departments at Brookhaven National Laboratory and the staff of the other PHENIX participating institutions for their vital contributions. We acknowledge support from the Office of Nuclear Physics in the Office of Science of the Department of Energy, the National Science Foundation, Abilene Christian University Research Council, Research Foundation of SUNY, and Dean of the College of Arts and Sciences, Vanderbilt University (U.S.A), Ministry of Education, Culture, Sports, Science, and Technology and the Japan Society for the Promotion of Science (Japan), Conselho Nacional de Desenvolvimento Científico e Tecnológico and Fundação de Amparo à Pesquisa do Estado de São Paulo (Brazil), Natural Science Foundation of China (P. R. China), Ministry of Education, Youth and Sports (Czech Republic), Centre National de la Recherche Scientifique, Commissariat à l'Énergie Atomique, and Institut National de Physique Nucléaire et de Physique des Particules (France), Bundesministerium für Bildung und Forschung, Deutscher Akademischer Austausch Dienst, and Alexander von Humboldt Stiftung (Germany), Hungarian National Science Fund, OTKA (Hungary), Department of Atomic Energy and Department of Science and Technology (India), Israel Science Foundation (Israel), National Research Foundation and WCU program of the Ministry Education Science and Technology (Korea), Physics Department, Lahore University of Management Sciences (Pakistan), Ministry of Education and Science, Russian Academy of Sciences, Federal Agency of Atomic Energy (Russia), VR and Wallenberg Foundation (Sweden), the U.S. Civilian Research and Development Foundation for the Independent States of the Former Soviet Union, the US-Hungarian Fulbright Foundation for Educational Exchange, and the US-Israel Binational Science Foundation.

[1] K. Adcox et al. (PHENIX Collaboration), Nucl. Phys. A **757**, 184 (2005).
[2] J. Adams et al. (STAR Collaboration), Nucl. Phys. A **757**, 102 (2005).
[3] B. B. Back et al. (PHOBOS Collaboration), Nucl. Phys. A **757**, 28 (2005).
[4] I. Arsene et al. (BRAHMS Collaboration), Nucl. Phys. A **757**, 1 (2005).
[5] K. Adcox et al. (PHENIX Collaboration), Phys. Rev. Lett. **88**, 022301 (2002).
[6] S. S. Adler et al. (PHENIX Collaboration), Phys. Rev. Lett. **91**, 072301 (2003).
[7] J. Adams et al. (STAR Collaboration), Phys. Rev. Lett. **91**, 172301 (2003).
[8] M. He, R. J. Fries, and R. R., Phys. Rev. C. **86**, 014903 (2012).
[9] R. Sharma, I. Vitev, and B.-W. Zhang, Phys. Rev. C. **86**, 014903 (2012).
[10] W. A. Horowitz and M. Gyulassy, J. Phys. G **35**, 104152 (2008).
[11] Y. L. Dokshitzer and D. E. Kharzeev, Phys. Lett. B **519**, 199 (2001).
[12] A. Adare et al. (PHENIX Collaboration), Phys. Rev. C **84**, 044905 (2011).
[13] A. Adare et al. (PHENIX Collaboration), Phys. Rev. Lett. **109**, 242301 (2012).
[14] H. Agakishiev et al. (STAR Collaboration), Phys. Rev. .D **83**, 52006 (2011).
[15] B. e. a. Abelev (ALICE Collaboration), Phys. Rev. D **86**, 112007 (2012).
[16] D. Thomas (ALICE Collaboration) (2013), arxiv:1312.1489.
[17] A. Adare et al. (PHENIX Collaboration), Phys. Rev. C **89**, 034915 (2014).
[18] A. Adare et al. (PHENIX Collaboration), Phys. Rev. C. **87**, 012011 (2013).
[19] A. Adare et al. (PHENIX Collaboration), Phys. Rev. Lett **111**, 202301 (2013).
[20] A. Adare et al. (PHENIX Collaboration), Phys. Rev. Lett. **103**, 082002 (2009).
[21] M. Aggarwal et al. (STAR Collaboration), Phys. Rev. Lett. **105**, 202301 (2010).
[22] A. Adare et al. (PHENIX Collaboration), Phys. Lett. B **670**, 313 (2009).
[23] K. Adcox et al. (PHENIX Collaboration), Nucl. Instrum. Methods A **499**, 469 (2003).
[24] (2013), adare, A. et al., (PHENIX Collaboration), arXiv:1310.4793.
[25] A. Adare et al. (PHENIX Collaboration), Phys. Rev. C **81**, 034911 (2010).
[26] J. A. Kamin (2012), ph.D. dissertation, Stony Brook Univerisity, USA.
[27] P. Crochet and P. Braun-Munzinger, Nucl. Instrum. Methods A **484**, 564 (2002).
[28] D. E. Groom et al., Euro. Phys. J. C **15** (2000).
[29] T. Sjostrand, S. Mrenna, and P. Z. Skands, PYTHIA *6.4 Physics and Manual* J. High Energy Phys. **05** (2006) 026.
[30] S. Frixione and B. Webber (2002), j. High Energy Phys. **06** (2002) 029.
[31] L. Aphecetche et al. (PHENIX Collaboration), Nucl. Instrum. Methods A **499**, 521 (2003).
[32] S. Adler et al. (PHENIX Collaboration), Phys. Rev. Lett. **98**, 172302 (2007).
[33] S. S. Adler et al. (PHENIX Collaboration), Phys. Rev. C **74**, 024906 (2006).
[34] A. Adare et al. (PHENIX Collaboration), Phys. Rev. C **84**, 044902 (2011).
[35] D. Sharma (2010), ph.D. dissertation, Weizmann Institute of Science, Israel.
[36] A. Adare et al. (PHENIX Collaboration), Phys. Rev. Lett. **107**, 142301 (2011).
[37] A. Adare et al. (PHENIX Collaboration), Phys. Rev. C **87**, 044909 (2013).
[38] J. Beringer et al. (Particle Data Group), Phys. Rev. D **86**, 010001 (2012).
[39] S. Frixione, P. Nason, and B. R. Webber, j. High Energy

Phys. **08** (2003) 007.
[40] G. Corcella and B. Webber, j. High Energy Phys. **01** (2001) 010.
[41] M. R. Whalley et al. (2006), HERA and the LHC - A workshop on the implications of HERA for LHC physics: Proceedings, C05-03-21.1, arxiv:hep-ph/0601012.
[42] K. Eskola, H. Paukkunen, and C. Salgado, j. High Energy Phys. **04** (2009) 065.